Journal of Materials Chemistry A

Accepted Manuscript

ROYAL SOCIETY OF CHEMISTRY

www.rsc.org/materialsA

Tables of Content (TOC)

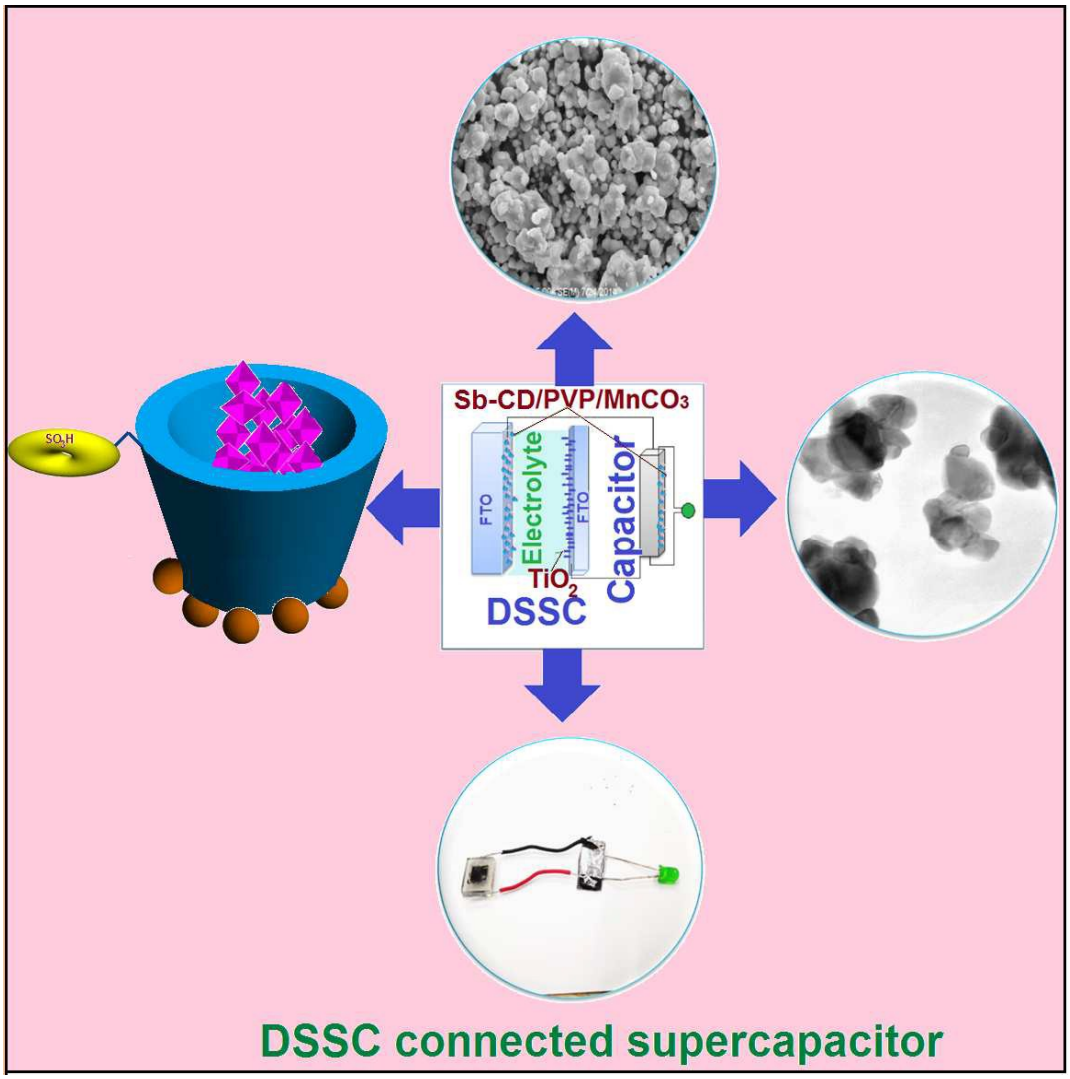

Journal of Materials Chemistry A

RSCPublishing

COMMUNICATION

Cite this: DOI: 10.1039/x0xx00000x

Novel high-temperature supercapacitor combined dye sensitized solar cell from sulfated β-cyclodextrin/ PVP/$MnCO_3$ composite

Received 00th January 2012,
Accepted 00th January 2012

DOI: 10.1039/x0xx00000x

www.rsc.org/

S.Selvam[a], B.Balamuralitharan[a], S.N.Karthick[a], A. Dennyson Savariraj[a]
K.V.Hemalatha[b], Soo-Kyoung Kim[a], Hee-Je Kim*[a],

Novel sulfated β-cyclodextrin/PVP/$MnCO_3$ composite has been synthesized for a parallel connected supercapacitor and dye-sensitized solar cell (counter electrode). β-cyclodextrin has sulfonated, thermally crosslinked with PVP, and incorporated with $MnCO_3$ nanoparticles. The composite electrode exhibited 202.6Fg^{-1} capacitance, 197.96$Whkg^{-1}$ energy density 5.57%η(DSSC) and 70% performance showed up to 200ºC with [BMI][TFSI] electrolyte.

Global research has attention to focus on development of sustainable energy storages and applications on conversion devices. The development of nanomaterial technology plays a vital role in energy harvesting and storage, because the characteristics of devices closely depend on the properties of the materials used.[1, 2] Single-electrode system for both supercapacitors (SC) and dye-sensitized solar cells (DSSCs) would be beneficial for smart energy storage and compact electronic devices. Polymer composite electrodes have attracted extensive consideration as the most suitable choice for fabricating compact, and laminated solid-state energy storage systems.

Electrochemical supercapacitors have drawn considerable attention in recent years because they have ability to provide high power density, fast charging, long cycle life, and low maintenance costs. SCs are passive and static electrical energy storage devices that deliver electrical energy with unusually high power densities compared to secondary batteries (10 $kWkg^{-1}$), but they use different mechanisms. Supercapacitors store electricity physically and Batteries store chemically by separating the positive and negative charges. Newer active materials such as transition metal oxides or electrically conducting polymers are required for high-performance capacitance supercapacitors.

In DSSCs, the counter electrode (CE) plays a vital role, since the tri-iodide shuttle species is reduced at the CE ($I_3+2e^- \rightarrow 3I^-$) by collecting the electrons from the external circuit. Usually, platinum (Pt) is used as a CE, but it limits the extensive application of DSSCs due to its corrosive behavior and high cost. In order to rectify these problems, low-cost and eco-friendly polymer-based or carbon-based CEs are necessary for instead of Pt CEs. New prepared composite CEs have new avenues such as, improved catalytic activity and high conductivity. Another important problem is the stability of electrolytes in a hot environment. An ionic liquid mixed electrolyte is suitable,[3-6] and we have tested the stability of such electrolytes in high thermal condition.

A very rare number of reports have been investigated and reported for DSSC combined SC. S.-H. Han group has reported the use of nanocrystalline tin oxide film electrodes at room temperature in photo anode of DSSC and SC. This report has been focused on the SC performance with 43.07Fg^{-1} of resulted specific capacitance.[7] A Ti wire substrate modified with titania nanotubes serve as DSSC and SC electrodes as the integrated "energy fiber" device has been reported. This report deals the modifications in photo anode of DSSC and the energy fiber obtained 2.73% of DSSC efficiency.[8] The shape selective nano TiO_2 has been used in SC and DSSC. The nano TiO_2 showed different specific capacitance results.[9]

A dye sensitized solar cell and a ruthenium oxide based electrochemical capacitor integrated system has been reported and it permits direct storage of energy generated by sunlight within a single optoelectronic microelectrochemical device. It utilizes three planar electrodes arranged sequentially to include a polymer hole as conductor (poly-(3-hexylthiophene-2,5-diyl)), between the titanium oxide photo anode modified with dye (E)-3-(5-(4-(Bis(20,40-dibutoxybiphenyl-4-yl)amino)phenyl)thiophen-2-yl)-2-cyanoacrylic acid (D35) and the intermediate silver electrode as well as two hydrous ruthenium oxide layers. This report has been achieved 0.8% efficiency for DSSC and 400 Fg^{-1} of specific capacitance for SC.[10]

The double-layer ZnONS/NP film also was used as the semiconducting film in the photo anode of a DSSC and capacitor and this report mainly focused on DSSC and 4.65% of efficiency obtained.[11] N. Bagheri groups have reported a DSSC based on the metal-free organic sensitizer and the cobalt (II, III) polypyridyl electrolyte was integrated within an asymmetric capacitor utilizing

cobalt-doped nickel oxide and activated carbon. The DSSC exhibited 4.6% of and 46Fg^{-1} specific capacitance.[12] Chen et al., to realize photoelectric conversion wire for energy storage and exhibits storage efficiency of 1.5%. A flexible device has reported to realize both photoelectric conversion and energy storage by using aligned MWCNT films. The integrated device exhibits a good photoelectric conversion. H. Sun group has reported a wire shaped energy wire (CNT) exhibited 6.58% of efficiency and specific capacitance of 85.03 $mFcm^{-1}$. A spinnable CNT array energy wire also exhibited 1.83% efficiency.[13-17] From these survey the DSSC and SC combined fabrications are classified as integrated energy wire, printable photo-supercapacitor, energy fiber, and energy films. There is no reports on parallel connected DSSC combined SC for high thermal operations. Based on the upstairs, a high performance electrode required for both DSSC and SC in parallel connection. Also very rare focus available for high thermal stability counter electrode for DSSC connected supercapacitor.

An eco-friendly polymer β-cyclodextrin has selected for this work, which is a cellulose-based polymer with properties of functional modification and thermal stability. However, bio-sourced products still expose future energy resource systems as wearable devices and these composite polymers exhibit catalytic activity.[18] A multi-functional polymer Poly-N-vinyl-2-pyrrolidone(PVP) has used in this work, it is a synthetic, non-toxic, water-soluble polymer which has been used in various fields like film formers, protective colloid and suspending agents, dye-receptive agents, binders, stabilizers, detoxicants, and complexing agents. PVP can be crosslinked by heating in air at 150ºC, by radiation, or by potassium persulfate. The important properties of hybrid material formation by PVP have been discussed in our previous report.[19] The most common interactions observed in PVP crosslinked polymer composites are hydrogen bonding, ionic, dipole, π-electron, and charge transfer complex interactions.[20]

The introduction of sulfonic groups increases the ion-exchange capacities. PVP cross-linking assists the ionic mobility with increasing mobile ion concentration, and it also increases the strength of the composite with the number of reactive ionic cluster sites. The selection high thermal stability electrolyte that is ionic liquids also played an important role. ILs are composed of a cation (imidazolium) and an anion (Sulfate, Borate, Phosphate, etc.) are organic salts that are liquid around room temperature. ILs are employed as good electrolytes in conducting polymers due to their good electrical conductivity, heat stability, and good corrosive resistance. ILs as permanent conductivity enhancers in polymeric films produced improved electrical performance.[21-23] We have demonstrated this novel route as a common electrode material for both DSSC and SC with high thermal stability. The combination of such materials could form high-performance SC and DSSC, which are cost-effective for applications where the development and consistency of the storage devices are important. A sulfated β-cyclodextrin/PVP/$MnCO_3$ composite has believed to provide clean energy for a long time even in hot environments.

A new technique was used for the synthesis of metal carbonates from potassium permanganate and mixing solvents such as methanol with DMF. The solvent proportion is adjusted for mono-dispersed crystalline $MnCO_3$ with rhombohedra morphologies. The $MnCO_3$ nanoparticles were prepared by $KMnO_4$ (0.1mm) with a mixed solvent (25mL) composed of methanol and DMF (N, N-dimethylformamide). This mixture was kept in a 33mL stainless-steel autoclave at 180ºC for 24 h.[24]

β-cyclodextrin was sulfonated using H_2SO_4 at a temperature of 0ºC, which was based on our previous report.[25] The synthesized sulfated β-cyclodextrin (Sb-CD) was thermally crosslinked with PVP. This Sb-CD/PVP composite was incorporated with various weight percentages (wt%) of $MnCO_3$, which were denoted as S1=0.5 wt%, S2=1.0 wt% and S3=1.5 wt%. The prepared Sb-CD/PVP/$MnCO_3$ composite electrodes were fabricated as a CE for a DSSC and also as a storage electrode for a SC. The DSSC and SC was connected in parallel, and ionic liquid containing 1-butyl-3-methylimidazolium bis (trifluoromethylsulfonyl)imide [BMI][TFSI] was used as the electrolyte. The efficiency of DSSC was checked under a solar simulator. The performance of DSSC and capacitance were measured up to 200ºC.

The XRD pattern of the prepared $MnCO_3$ presents peaks (102), (104), (110), (113), (202), (116), (122), and (300) indexed to the crystal structure (Fig. 1.a (i)). The common crystal growth model cleavage (104) peak with a sharp (012) peak represent rhombohedra, which is very rare (JCPDS Card: 83-1763)[26]. Fig 1.a (ii) shows the diffraction pattern, which is probably due to the crystalline cellulosic structures of Sb-CD. PVP indicates an amorphous nature with low crystallinity in the XRD pattern (Fig. 1.a (iii)). The XRD results indicate that the crystalline structures of cellulose[27] are mostly disrupted by PVP and $MnCO_3$ nanoparticles present in the composite (Fig. 1.a (iv)). Most of the crystalline peaks indicate the $MnCO_3$ pattern. This is evidence for the incorporation of $MnCO_3$ nanoparticles with Sb-CD/PVP and also the miscibility of cellulosic chains in the synthesized composite (Supplementary information Fig 1. FTIR).

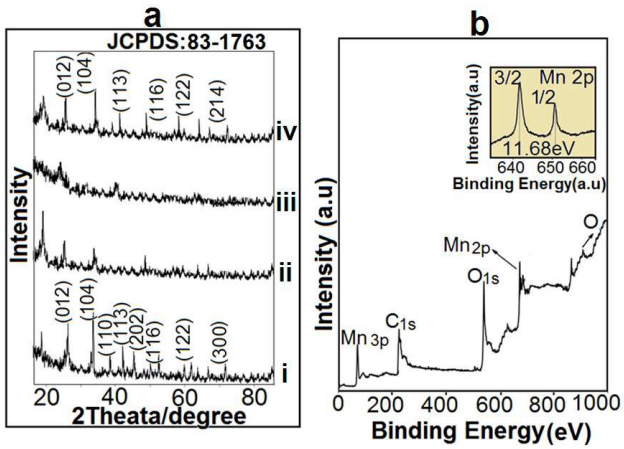

Fig. 1(a) XRD pattern of (i) $MnCO_3$, (ii) Sb-CD, (iii) PVP and (iv) Sb-CD/PVP/$MnCO_3$; (b) XPS spectrum of $MnCO_3$

The XPS spectrum indicates the presence of Mn, O, and C as the main constituents (Fig. 1.b). The peaks of Mn 2p1/2 and

Mn 2p3/2 are centered at 653.4 and 642 eV, respectively, with a spin energy separation of 11.68 eV. This result is in coinciding with reported data for $MnCO_3$. The solvent ratio and $KMnO_4$ may also react to form $MnCO_3$.[28, 29]

$$5CH_3OH + 4MnO_4^- + 12H^+ \rightarrow 4Mn^{2+} + 11H_2O + 5HCOOH \quad \ldots 1$$

$$5HCOOH + 2MnO_4^- + 6H^+ \rightarrow 2Mn^{2+} + 5CO_2 + 8H_2O$$

$$2(CH_3)_2 - N - CHO + 2MnO_4^- + 6H^+ \rightarrow 5(CH_3) - NH +$$

$$2Mn^{2+} + 5CO_2 + 3H_2O \quad \ldots\ldots 2$$

$$2MnO_4^- + Mn^{2+} \rightarrow Mn_3O_4 \quad \ldots\ldots 3$$

$$CO_2 + H_2O \rightarrow CO_3^{2-} + 2H^+$$

$$Mn^{2+} + CO_3^{2-} \rightarrow MnCO_3 \quad \ldots\ldots 4$$

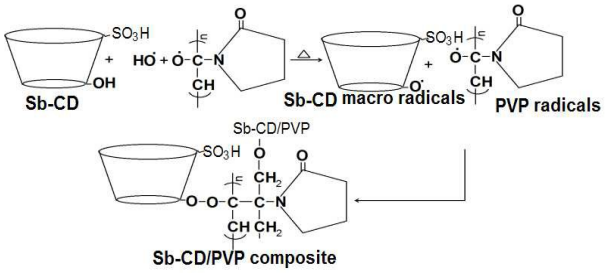

$\ldots 5$

Fig 2.a1 shows the $MnCO_3$ nanoparticles obtained from pure mixed solvents. It can be seen that the morphology and the size are not uniform, and the particles reunite badly, which implies a rapid nucleation process. The particle size was controlled by the microemulsion, which restrains the growth of $MnCO_3$ nanoparticles. TEM images also confirm the shape with size ranging from 30 nm to 100 nm (Fig. 2.a2). Due to the intense redox in the pure solvent, there is a minor aggregation of Mn_3O_4 followed by a side reaction (eqn. 1 to 4) when the Mn^{2+} ratio is higher at the initial stage of the polymer layer deposition on surface of the nanoparticles. The controlled morphology with size also depends on the solvent proportions.

A TEM image of the Sb-CD/PVP/$MnCO_3$ composite is also confirms the polymer layer deposition, and each particle shows a cavity and the incorporation of Sb-CD showed in fig 2.e. [30, 31] Sb-CD and PVP molecular interactions are clearly visible in the SEM image of the Sb-CD/PVP composite (Fig.2.b1). The reason for the agglomerated structure is that the PVP may acts as a film-forming agent. The PVP thermal crosslinking and structural changes are assumed in eqn. 5, and this crosslinking with cellulosic polymer reaction mechanism has been discussed in our previous report.[19] These structural changes are due to the hydrogen bonding interactions between the hydroxyl groups of the polymer components.[32] The $MnCO_3$ nanoparticles and crosslinked polymers exhibit bulk composite structures as mentioned in Fig. 2.(c1&c2).

Fig. 3.a represents the cyclic voltammetry studies of synthesized composites Sb-CD, SbCD/PVP, $MnCO_3$, S1 (0.5 wt% $MnCO_3$), S2 (1.0 wt% $MnCO_3$), and S3 (1.5 wt% $MnCO_3$) recorded at a scan rate of 10 mV/s. In this CV results, Sb-CD and Sb-CD/PVP polymer composite exhibited maximum covered typical oxidation and reduction peaks. The CV curves of the S1, S2, and S3 electrodes clearly seen that all voltammograms have nearly rectangular in shape, revealing the perfect electrochemical capacitive behavior of the Sb-CD/PVP/$MnCO_3$. All the curves of the electrode S1, S2, and S3 show no obvious peaks, indicating that these electrodes are charged and discharged at a pseudo constant rate over the complete voltammetric cycle and the surface process that is the adsorption/desorption of ions.

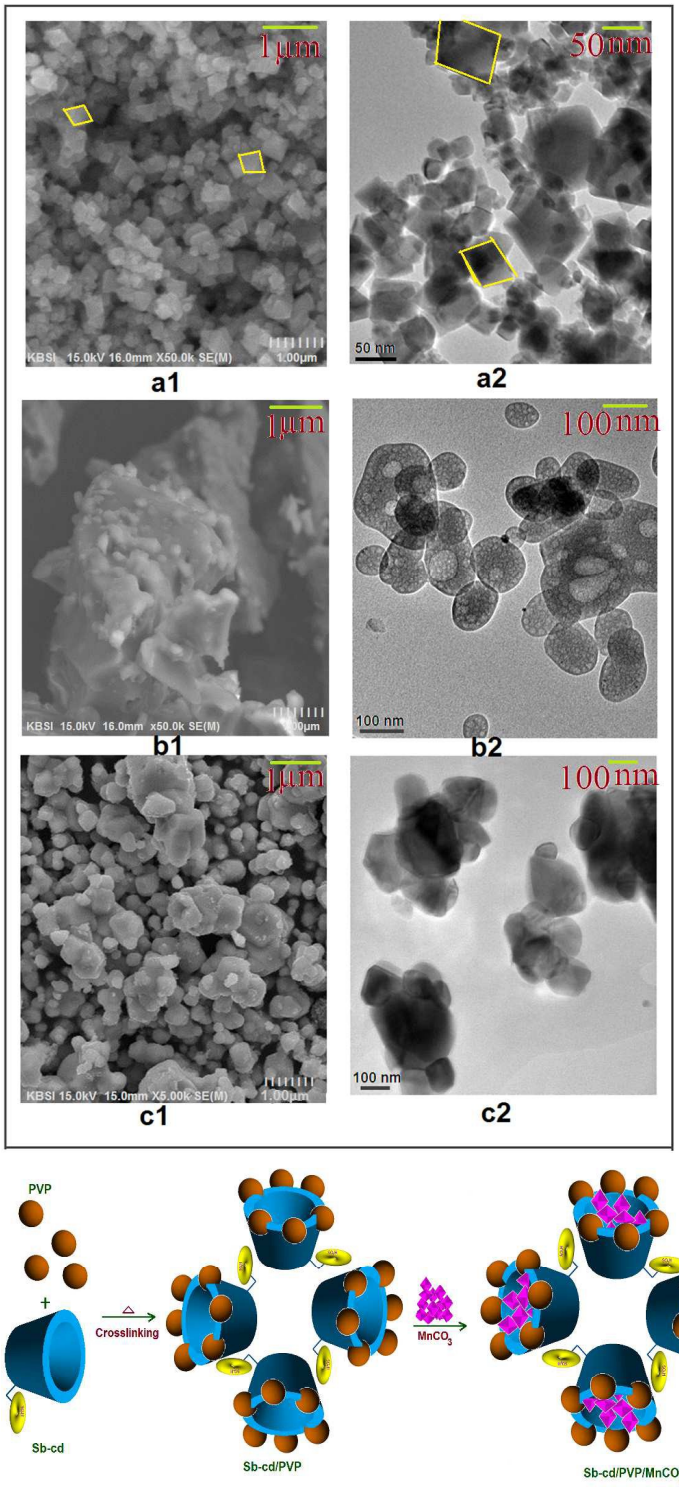

Fig.2(a1&a2) SEM and TEM images of $MnCO_3$, (b1&b2)Sb-CD/PVP, (c1&c2) Sb-CD/PVP/$MnCO_3$ and (e) Graphical representation of Sb-CD/PVP/$MnCO_3$ composite synthesis.

In contrast, an obvious distortion from the rectangular shape in the CV curves for Sb-CD/PVP/$MnCO_3$ electrodes. This phenomenon can be explained from the view of the ionic motion in electrolyte to electrode solid phase. It is evident that mass loading of $MnCO_3$ creates the different thickness of the electrodes and the S3 electrode is much thicker than that of the S1 and S2 electrodes. In the range of the applied scan rates, ions have enough time to reach the surface of $MnCO_3$ for the electrode S1 and S2 for its thin thickness. The absorption/desorption reaction can occur favourably. But in the case of S3 electrode, it can be speculate that a longer distance of ionic motion. Hence S3 electrode exhibits lower capacitance than S2 electrode. In addition, this substantial electrochemical performance could be increased by sulfonated polymers, functional groups of PVP, and these functional groups are creating electrochemically active catalyst area on electrode surface. Also the presences of polymers complement the metal ions in terms of boosting the capacitance.[33-36]

Fig. 3. b shows the CV curves of S2 electrode at increased from 10mV/s to 200mV/s and this S2 composite exhibits no obvious deviation rectangular shape, which could be attributed to the influence of pseudocapacitance with $MnCO_3$. The area in the CV curve of the composite electrode shows an incredible improvement compared to electrodes with $MnCO_3$ and Sb-CD/PVP alone. The reason for charge storage in the prepared composites explained by two mechanisms, one is the adsorption-desorption and other is intercalation-deintercalation of protons and/or alkali metal ions on the surface of the oxide respectively. From the $MnCO_3$ with concomitant reduction-oxidation of the Mn ions.[37, 38] The oxidation state of Mn in $MnCO_3$ is +2, so the possibility of charge storage by the second mechanism is very improbable. However, high capacitance may also be obtained by increasing amount of $MnCO_3$ particles.

Nyquist plots of the $MnCO_3$, Sb-CD/PVP, and the S1, S2, and S3 composites are shown in Fig 3(c). All the plots show a semicircular arc in the high-frequency region and a straight line in the low-frequency region. The diameter of the semicircle in the high-frequency region is attributed to the charge-transfer resistance of the electrode (Rct). There are several accumulated polymers noticed on the external surface of composites electrode as exposed in the SEM and TEM. These accumulated Sb-CD/PVP polymers on the outer surface decrease to contact with the electrolyte fully. The interaction between the aggregated polymer composite and electrolyte is weak that it makes few contributions to charge accumulation. Moreover, the accumulated polymer on the outer surface may plug up the pores and block the diffusion of electrolyte, which prevents the interaction of active material with the electrolyte. This may increase resistance effects in this composite electrode at high frequency region. The straight line in the low-frequency region arises for S1, S2, and S3 due to the pseudo capacitance (Cp). The high-frequency intercept with the real axis is related to the equivalent series resistance (Rs), which contains the resistance of the bulk electrolyte solution, the inherent resistance of the active material, and the contact resistance at the active material/current collector. The steep slope corresponds to efficient ions penetration between electrode and electrolyte.

In the equivalent circuit, a solution resistance (R_S) is connected in series with a double layer capacitance (C_{DL}), and the C_{DL} is connected in parallel with the charge transfer resistance (R_{ct}) and pseudocapacitance (C_P).

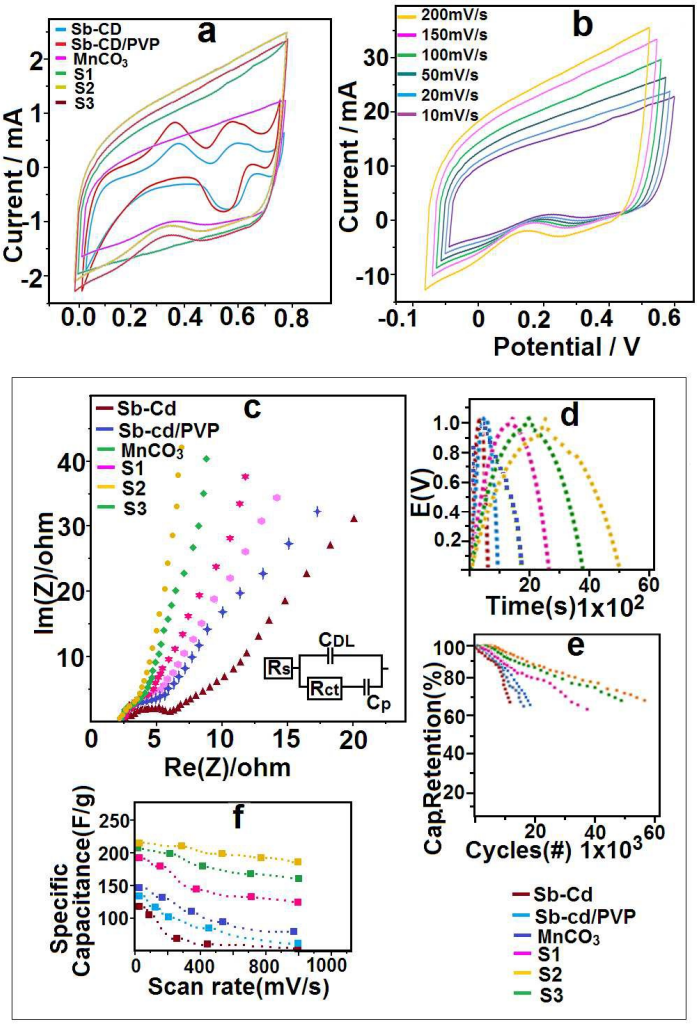

Fig. 3(a) Cyclic Voltammetry of S1, S2 and S3 electrodes, (b) Cyclic Voltammetry of S2 with increasing scan rate, (c) Nyquist plots of the impedance spectra, (d) charge-discharge curve of composites and (e) Cycling performance and (f) Specific capacitance for S1, S2 & S3 composite electrodes.

The parallel R_{ct} and C_{DL} configuration accounts for the semicircular feature, while C_P accounts for the steep line. For supercapacitors, the majority of the capacitance is available only at low frequency, so attention should be paid to keeping the impedance data in this range.[39] The charge-discharge curves of the S1, S2 and S3 composite electrodes exhibited pseudo capacitance performance as, since they deviate from linear shapes, as shown in Fig 3.d. This can also be confirmed from the skewed triangle shape of the charge-discharge curves of composites and the increased discharge time compared with the symmetrical triangle of the curves with limited discharge time for composite electrodes. The capacitance could also be calculated from the galvanostatic discharge curves using the following equation 6.

$$C = \frac{I\Delta t}{m\Delta V} \quad .....6$$

Where I (A) is charge or discharge current, Δt (s) is the time for a full charge or discharge, m (g) indicates the mass of the active material, and ΔV represents the voltage change after a full charge or discharge.[40] The $MnCO_3$ exhibited 126.2Fg^{-1} of capacitance and the S2 (Sb-CD/PVP/$MnCO_3$) composites possess the highest capacitance of 202.6Fg^{-1}. Moreover, these types of composites conserve a minimum 65% from their initial capacitance (Fig 3.e).

The intended specific capacitance (SC) decreased with increasing scan rate (Fig 3.f). At low scan rates, the ions from the electrolytes have enough time to adsorb/desorb at the inner and outer surfaces of the active material. At higher scan rates, the ions access only the outer surface of the active material due to the limited accessible time from the electrolyte. Hence, low SC is observed at high scan rates. From these results, it is confirmed that when the scan rate increases, the capacitance of all samples decreases, and in the high frequency region, the supercapacitors behave like a mild resistor, which indicates that the electrolyte ions cannot penetrate into the micropores under increased scan rates or high frequencies.

The corresponding supercapacitor was also fabricated in a two-electrode system with [BMI][TFSI] ionic liquid as the electrolyte. The S2 composite was mixed with carbon black, which was made into a slurry with a few drops of poly(tetrafluorethylen). This was coated on a nickel mesh and dried at 90ºC. The CE was prepared by coating S2 composite on FTO glass plate as in our earlier reports (Fig. 4.b).[41, 42] The DSSC was fabricated with a dye-absorbed TiO_2 photo anode and iongel electrolyte[43] ([BMI][TFSI] ionic liquid with KI and I_2). The fabricated supercapacitor was parallel connected with the prepared DSSC (Fig. 4.a). The fabricated cell was placed under 1 sun solar simulator (Fig.4.b & c) and the exhibited efficiency was checked. The storage performance also analysed for supercapacitor after cut off the light simulation (Fig.4d). The schematic structure of supercapacitor and DSSC showed in fig.4e and f.

The fabricated supercapacitor and DSSC cell was placed in an electric oven at 25˚C for 2 h for thermal stability analysis.[33] The temperature was increased as follows 25º, 35º, 50º, 75º, 100ºC and then cell was put in an electric furnace at150ºC and 200 ºC. The each increased temperature analysed values were summarized in fig. 4g and table 1with photovoltaic parameters of DSSCs.

From photovoltaic analysis the Sb-CD/PVP/$MnCO_3$ composite polymer showed good catalytic activity. In the case of S2 counter electrode exhibited a good short-circuit current density (Jsc) of 11.36 $mAcm^{-2}$; however, the fill factor is 68.2% and efficiency is 5.57%. By comparison, the Pt counter electrode DSSC showed 6.71 % of efficiency, which is nearly closed by the Sb-CD/PVP/$MnCO_3$ counter electrode under the same conditions. The photovoltaic results showed good catalytic activity as CE catalysts for the I_3^- reduction in DSSC. The Sb-CD/PVP/$MnCO_3$ counter electrode has S, O and N atoms in its structure, which may be help for the catalytic activity. It also is clear that the host metal ($MnCO_3$) should be incorporated with the alien atoms (C, S or N) exhibit good catalytic behavior distinct from the metal hosts and that their activity patterns closely resemble those of Pt. The incorporation with PVP heteroatoms also enhances the electro catalytic activity in the counter electrode, which results in higher J_{sc} and FF, there by resulting in higher conversion efficiency.

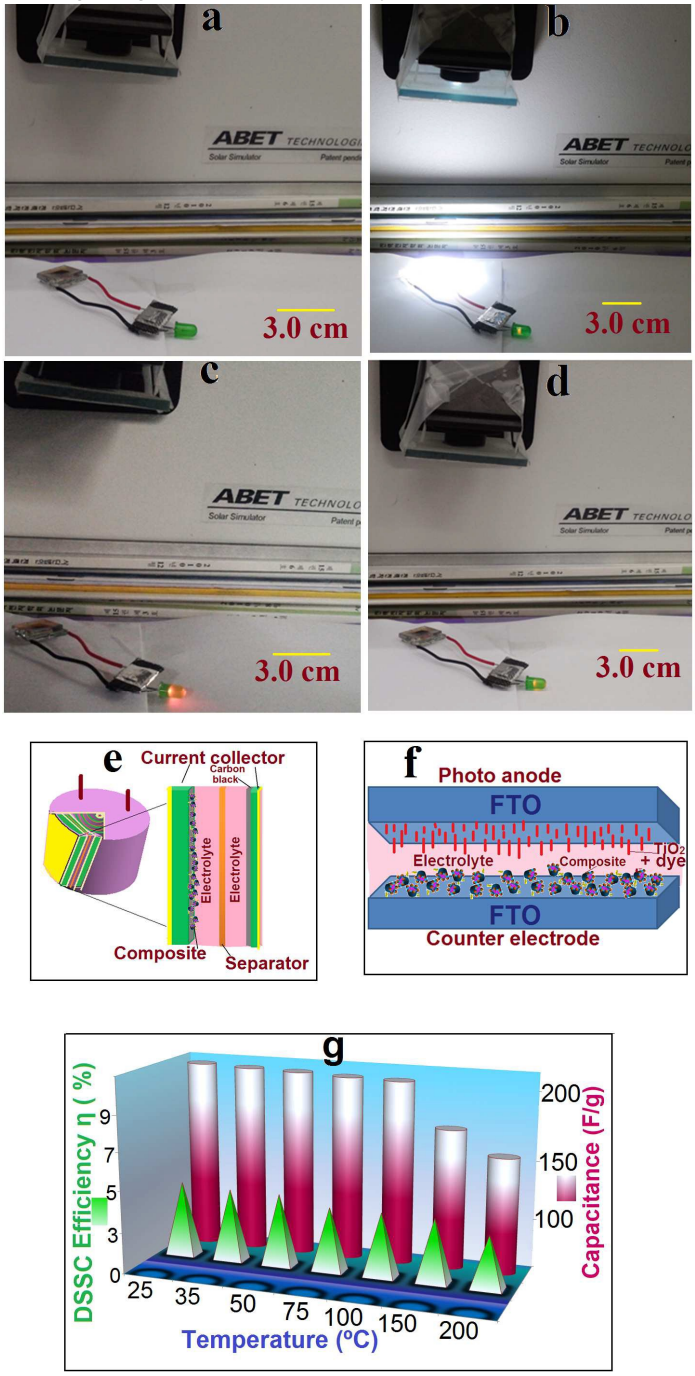

Fig.4.a. Fabrication supercapacitor combined DSSC for stability and efficiency performance under solar simulation before solar light simulation; (b) under light simulation; (c) cut-off light simulation initial; (d) after 4 minutes cut off simulation and (e&f). Structure of supercapacitor and counter electrode and (g) High thermal stability analysis of S2 electrode.

Besides the presence of heteroatom of PVP including nitrogen, sulfonated β-cyclodextrin and carbon matrix are favor the adsorption and subsequent reduction of triiodide. Also the co-doping of N and S atoms enhanced the asymmetric spin density as well as the charge density, which are responsible for the electro catalytic activities has been reported that.

Table 1: DSSC performances of Sb-CD/PVP/$MnCO_3$ CE under 1 sun illumination

Samples.	J_{sc} ($mAcm^{-2}$)	V_{oc} (V)	FF (%)	ɲ (%)
S1(0.5wt% of $MnCO_3$)	7.60	0.70	53.9	2.89
S2(1.0wt% of $MnCO_3$)	11.36	0.72	68.2	5.57
S3(1.5wt% of $MnCO_3$)	7.61	0.72	69.8	3.82
Pt	12.49	0.75	71.8	6.71

However it is also evident that the electronic structure of the host metal ($MnCO_3$) should be modified by the alien atoms (i.e., C or N) induced the electron transfer process, the direction (i.e., host metal to interstitial atom or interstitial atom to host metal) and extent of electron transfer has been debated. In addition, the catalytic activity can be also affected significantly by the particle size, mass load and crystal structure, etc., [44-47]

Table 2: Comparison of high thermal stability of supercapacitor and dye sensitized solar with literature.

High temperature operated Supercapacitor

Ref. No.	Electrode	Electrolyte	Temp. (°C)	Cap. (Fg^{-1})
This work	$MnCO_3$	[BMI][TFSI]	200	65
This work	Sb-CD/PVP/$MnCO_3$	[BMI][TFSI]	200	152
48	F-Polybenzoxazoles	Polyimide	250	31
49	RGO	[BMI][TFSI]	200	50
50	SWNT	$TEABF_4$/PC	100	32
51	Activated carbon	BuCN	80	125
52	Activated carbon	[Pyrr][NO_3]	80	117
52	Activated carbon	[C_2mIM][TFSI]	60	17

High temperature operated dye sensitized solar cells

Ref. No.	Counter Electrode	Photo anode	Electrolyte	Temp. (°C)	Eff. (ɲ%)
This work	Sb-CD/PVP/$MnCO_3$	TiO_2	Iodine/ [BMI][TFSI]	200	3.9
53	Pt - (hydrogen hexachloroplatinate (IV) hydrate)	TiO_2	Iodine/ [DMPII]	120	4.8
54	Pt-(H_2PtCl_6)	TiO_2	Iodine/ acetonitrile	120	1.7
55	Pt - (hydrogen hexachloroplatinate (IV) hydrate)	TiO_2	Iodine/ [CEMim]	100	1.9
56	Pt- (Chloroplatinic acid embedded Titanium plate)	TiO_2	Iodine/ additives	85	5.5

[Pyrr][NO_3]-pyrrolidiniumnitrate;[C_2mIM][TFSI]-1-ethyl-3-methy limidazolium bis[(trifluoromethyl)sulfonyl]imide; BuCN-Butyronitrile; SWNT-single wall carbon nanotube; $TEABF_4$/PC : tetraethylammonium tetrafluoroborate-polypropylene carbonate; [DMAp]2-(dimethylamino)-pyridine; [CEMim]5-chloro-1-ethyl- 2-methylimidazole.

Table 2 deals with the comparison of this composite value with already reported. So far, no report was published in high temperature supercapacitor combined with dye sensitized solar cell. Hence the comparison report was tabulated separately for supercapacitor and dye sensitized solar cell. Sb-CD/PVP/$MnCO_3$ electrode used supercapacitor exhibited 152 Fg^{-1} of capacitance at 200°C which shows a higher capacitance performance than the other reported results. This composite CE also exhibited 3.9% of efficiency at 200°C with DSSC application. From literature, high efficiency of 4.9% at 120°C is already reported. But the operating temperature is lower than our present report. And based on the previous reports the Sb-CD/PVP/$MnCO_3$ composite electrode showed some notable improvement in the performance.

Conclusions

In summary, we have successfully fabricated Sb-cd/PVP/$MnCO_3$ composite electrodes for a parallel connected supercapacitor and a DSSC (CE). In this work we have used eco-friendly polymers as β-CD, PVP and a simple method introduced for high-temperature electrodes with ionic liquid iongel electrolyte. The conductive composite electrode with 1.0Wt% of $MnCO_3$ (S2) of has produced efficient performance for supercapacitor and also good counter electrode for dye sensitized solar cell. This electrode exhibited a good photo conversion efficiency of 5.57% and a highest specific capacitance of 202Fg^{-1} and this performance has maintained up to 25ºC to 75ºC. In high thermal treatment at 200˚C, this electrode retains 152 Fg^{-1} of capacitance with 3.9% of DSSC efficiency. Also the Sb-cd/PVP/$MnCO_3$ composite has exhibited 197.96 $Whkg^{-1}$ of energy density and 86.06$kWkg^{-1}$ of power density. This type of composite may be suitable electrode materials as energy storage devices in hot environment.

Acknowledgements

The first author would like to thank the "BK 21 PLUS, Creative Human Resource Development Program for IT Convergence, Pusan National University, Busan, South Korea for its financial support. In addition, this research was supported by the MOTIE (Ministry of Trade, industry & Energy), Korea, under the Industry Convergence Liaison Robotics Creative Graduates Education Program supervised by the KIAT (N0001126).

Notes and references

[a]School of Electrical Engineering, Pusan National University, Gumjeong-Ku, Jangjeong-Dong, Busan 609-735, South Korea. E-mail: heeje@pusan.ac.kr; sselvam222@gmail.com.

[b]Department of Chemistry, Coimbatore Institute of Technology, Coimbatore, Tamil Nadu, India. E-mail: hemaac@gmail.com

†Electronic Supplementary Information (ESI) available: Materials used, Characterization techniques, FTIR spectra, EDX analysis, Impedance and fitting tale for DSSC and SC, J-V curve for DSSC, TGA studies and calculations for Capacitance, Energy density and power density details of any supplementary information available should be included here].

1 N. A. Kumar and J.B. Baek, Chem. Commun., 2014, 50, 6298-6308.
2. J. Liu, D. Qian , H. Feng, J. Li, J. Jiang, S. Peng and Y. Liu, J. Mater. Chem. A., 2014, 2, 11372-11381.
3. H. Jiang, J. Mab and C. Li, J. Mater. Chem., 2012, 22, 16939-16942.
4. N. Singh, C. Galande, A. Miranda, A. Mathkar, W. Gao, A.L. Mohana, and P.M. Ajayan, Scientific Reports., 2012, 481, 2, 1-5.
5. P. Simon and Y. Gogots, Nature Materials., 2008, 7, 845- 854.
6. P. Leung, X. Li, C.P. Leo´n, L. Berlouis, C. T. J. Lowa and F.C. Walsh, RSC Adv., 2012, 1-32,DOI: 10.1039/c2ra21342g.
7. R.S. Mane, J. Chang, D. Hama, B.N. Pawar, T. Ganesh, B.W. Cho, J.K. Lee, S.-H Han, Curr Appl Phys., 2009, 9, 87-91.
8. X.Chen, H.Sun, Z.Yang, G.Guan, Z.Zhang, L.Qiu, H.Peng, J. Mater. Chem. A., 2014, 2, 1897-1902.
9. U. Nithiyanantham, and S.Kundu, RSC Adv., 2014, 4, 35659-35672.
10. M.S-.Nuckowska, K. Grzejszczyk, P.J. Kulesza, L. Yang, N.Vlachopoulos, L.Häggman, E.Johansson, A.Hagfeldt, J. Power Sources., 2013, 234, 91-99.
11. C.-W. Kung, H.-W. Chen, C.-Y.Lin, Y.-H. Lai, R.Vittal, K-C.Ho, Prog. Photovolt: Res. Appl., 2014, 22, 440-451.
12. N. Bagheria, A.Aghaei, M.Y.Ghotbi, E.Marzbanrad, N.Vlachopoulos, L. Häggman, M. Wang, G. Boschloo, A. Hagfeldt, M. S-Nuckowskaf, P. J. Kuleszaf, Electrochim Acta., 2014, 143, 390-397.
13. T. Chen, L. Qiu, Z. Yang, Z. Cai, J. Ren, H. Li, H. Lin, X. Sun and H. Peng. Angew. Chem. Int. Ed. 2012, 51, 11977-11980.
14. Z. Yang, L. Li, Y. Luo, R. He, L. Qiu, H. Lin and H. Peng. J. Mater. Chem. A, 2013, 1, 954-958.
15. Z. Zhang , X. Chen , P. Chen, G. Guan , L. Qiu , H. Lin , Z. Yang, W. Bai , Y. Luo and H. Peng. Adv. Mater. 2014, 26, 466-470
16. H. Sun, X. You, J. Deng, X. Chen, Z. Yang, P. Chen, X. Fang and H. Peng. Angew. Chem. Int. Ed. 2014, 53, 6664 -6668.
17. Z. Yang , J. Deng , H. Sun , J. Ren , S. Pan and H. Peng. Adv. Mater. 2014, 26, 7038-7042.
18. S. Nagarajan, P. Sudhagar, V. Raman, W. Cho, K. S. Dhathathreyan and Y.S. Kang, J. Mater. Chem. A., 2013, 1, 1048-1054.
19. S. Selvam, M. Sundrarajan, Carbohydr. Polym., 2012, 87, 1419-1424.
20. H.M. Fahmy, M.H. Abo Shosha and N.A. Ibrahim., Carbhydr. Polym., 2009, 77, 4, 845-850.
21. Y. Xue, X. Zhai and M. Yu, Mater. Res. Bull., 2012, 47,393-399.
22. X. Liang, F. Zhang, W. Feng, X. Zou, C. Zhao, H. Na, C. Liu, F. Suna and G. Zhu. Chem. Sci., 2013, 4, 983-992.
23. S. Sun, J. Lang, R. Wang, L. Kong, X. Lia and X. Yan, J. Mater. Chem. A., 2014, 2, 14550-14556.
24. H.K. Lee, D. Sakemi, R. Selyanchyn, C.G. Lee and S.W. Lee, Appl. Mater. Interfaces., 2014, 6, 57-64.
25. S. Selvam, R. R. Gandhi, J. Suresh, S. Gowri, S. Ravikumar, M. Sundrarajan. Int J Pharmaceut., 2012, 434, 2, 366-374.
26. P. Pal, A. K. Giri, S. Mahanty and A. B. Panda, Cryst Eng Comm., 2013, 1-10, DOI: 10.1039/C4CE01334D.
27. S.Y. Lee, and Y. Lee. Macromol. Symp., 2006, 242, 126-130.
28. J. Wei, Y. Liu, Y. Ding, C. Luo, X. Dua and J. Lina. Chem. Commun., 2014, 50, 11938-11941.
29. J. Yuan, J. Zhu, H. Bi, Z. Zhang, S. Chen, S. Liang and X. Wang, RSC Adv., 2013, 3, 4400-4407.
30. X. Duan, T.Kim and W. Zheng., Commun., 2010, 46, 7133-7135.
31. S. Devaraj, and P. Balaya., J. Mater. Chem. A, 2014, 2, 4276-4281.
32. C.X. Liu and R.B. Bai, J. Membr. Sci., 2005, 267, 68-77.
33. P. A. Mini, A. Balakrishnan, S.V.Nair and K. R. V. Subramanian, Chem. Commun., 2011, 47, 5753-5755.
34. R. Paisal, R. Martínez, J. Padilla and A.J. F. Romero. Electrochimica Acta., 2011, 56, 6345- 6351.
35. C. Yang, J. Shen, C. Wang, H. Fei, H. Bao and G. Wang, J. Mater. Chem. A., 2014, 2, 1458-1464.
36. H.S. Park, S.J. Ko, J.S. Park, J.Y. Kim and H.K. Song. Scientific Reports., 2013, 3, 2454, 1-5, DOI: 10.1038/srep02454.
37. J. Hou, Y. Li, M. Mao, L. Ren and X. Zhao, Appl. Mater. Interfaces., 2014, 6, 14981-14987.
38. X. Duan, J. Ma, J. Lian, T. Kim and W. Zheng, Chem. Commun., 2010, 46, 7133-7135.
39. R. B. Rakhi, W. Chen and H. N. Alshareef, J. Mater. Chem., 2012, 22, 5177–5183.
40. R. Madhu, K.V. Sankar, S.M.Chen and R. Kalaiselvan. RSC Adv., 2014, 4, 1225-1233.
41. Hee-Je Kim, C.V. V. M. Gopi, M. V.Haritha, S.-K. Kim, Dalton Trans., 2015, Advance Article, DOI: 10.1039/C4DT03063J, 1-9.
42. Hee-Je Kim, D.J. Kim, S. S. Rao, A. D. Savariraj, K.S-K. Kim, K. Prabakar. Electrochimica Acta., 2014, 127, 427-432.
43. J.L. Bideau, and A. Vioux., Chem. Soc. Rev., 2011, 40, 907-925.
44. M. Wu, X. Lin, Y. Wang, L. Wang, W. Guo, D. Qi, X. Peng, M. Grätzel and T. Ma, J. Am.Chem. Soc. 2012, 134, 3419-3428
45. A.G. Kannan, J. Zhao, S. G. Jo, Y. S. Kang and D. –W. Kim, J. Mater. Chem. A, 2014, 2, 12232-12239
46. J. Liang, Y. Jiao, M. Jaroniec and S. Z. Qiao, Angew. Chem., Int. 2012, 51, 11496-11500.
47. I.I. Perepichka, M.A. Mezour, D.F. Perepichka and R. B. Lennox. Chem. Commun., 2014, 50, 11919-11921.
48. N.Venkat, T.D. Dang, Z.Bai, V.K. McNier, J.N. DeCerbo, B.H.Tsao, J.T. Stricker. Mater. Sci. Eng. B., 2010,168, 16-21.
49. R.S. Borges, A.L.M. Reddy, M.T.F. Rodrigues, H. Gullapalli, K. Balakrishnan, G.G. Silva, P.M. Ajayan. Scientific Reports., 2014, 2572, 1-6, DOI: 10.1038/srep02572.
50. C. Masarapu, and B. Wei, ACS Nano., 2009, 3, 8, 2199-2206.
51. V. Ruiz, T. Huynh, S.R. Sivakkumar, A. G. Pandolfo, RSC Advances., 2012, 2, 5591-5598.
52. M. Anouti, Phys. Chem. Chem. Phys., 2013, 15, 6539-6548.
53. F. Ghamouss, A. Brugère, J. Jacquemin, J. Phys. Chem. C., 2014, 118, 14107-14123.
54. H.S. Leea, S.H. Bae, Y. Jo, K.J. Kim, Y. Jun, C.H. Han, Electrochim Acta., 2010, 55, 7159-7165.
55. D. Högberg, B. Soberats, S. Uchida, M. Yoshio, L. Kloo, H. Segawa, T. Kato., Chem. Mater., Just Accepted Manuscript • DOI: 10.1021/cm503090z • Publication Date (Web): 21 Oct 2014, 1-7,
56. S. Noda, K. Nagano, E. Inoue, T. Egi, T. Nakashima, N. Imawaka, M. Kanayama, S. Iwata, K. Toshima, K. Nakada, K.Yoshino, Synthetic Met., 2009, 159, 2355-2357.

